Magneto-optic Kerr Effect Measurement of $TbMn_6Sn_6$ at mK Temperature

Dai-Qiang Huang(黄代强)[1†], Yang Wang(汪洋)[2†], He Wang(王贺)[2*], Jian Wang(王健)[1,3,4], and Yang Liu(刘阳)[1*]

[1]*International Center for Quantum Materials, Peking University, Beijing 100871, China*
[2]*Department of Physics, Capital Normal University, Beijing 100048, China*
[3]*Collaborative Innovation Center of Quantum Matter, Beijing 100871, China*
[4]*Hefei National Laboratory, Hefei 230088, China*

(Received 17 January 2024; accepted manuscript online 21 March 2024)

Novel electron states stabilized by Coulomb interactions attract tremendous interests in condensed matter physics. These states are studied by corresponding phase transitions occurring at extreme conditions such as mK temperatures and high magnetic field. In this work, we introduce a magneto-optical Kerr effect measurement system to comprehensively explore these phases in addition to conventional transport measurement. This system, composed of an all-fiber zero-loop Sagnac interferometer and *in situ* piezo-scanner inside a dilution refrigerator, operates below 100 mK, with a maximum field of 12 Tesla and has a resolution as small as 0.2 μrad. As a demonstration, we investigate $TbMn_6Sn_6$, where the manganese atoms form Kagome lattice that hosts topological non-trivial Dirac cones. We observed two types of Kerr signals, stemming from its fully polarized ferromagnetic ground state and positive charged carriers within the Dirac-like dispersion.

DOI: 10.1088/0256-307X/41/4/047801

Magneto-optical Kerr effect (MOKE) becomes increasingly important in condensed matter physics, especially in the study of quasi-two-dimensional systems such as thin films and interfaces.[1–5] The clock-wise (CW) and counter-clock-wise (CCW) circularly polarized light injected onto the sample surface drives the charges in the material to rotate accordingly. A magnetic field will give rise to an energy difference between the particles' CW and CCW orbital motions. In materials with spin-orbit coupling (SOC), it introduces an additional energy to these two motions through spin-polarizing electrons by the Zeeman effect. These energy differences lead to finite off-diagonal terms in the complex dielectric tensor $\hat{\varepsilon}_{xyz}$ which contributes to the magneto-optic effects.[6,7]

Recently, fragile electronic states in quantum materials that are stabilized by Coulomb interactions become of great interests.[8,9] To detect these rich physics that only appear at ultra-low temperature and high magnetic field, we built a MOKE measurement setup consisting of an all-fiber zero-loop Sagnac interferometer[10,11] and *in situ* piezo-scanner integrated inside a dilution refrigerator. Our system's geometry is designed for a polar Kerr signal where the light is injected perpendicular to the surface and is sensitive to the magnetization along the same direction. It can operate below 100 mK and inside magnetic field up to 12 T, and achieves below 0.2 μrad resolution. A scanning stage allows us to image the sample while keeping its temperature below 100 mK.

$TbMn_6Sn_6$ is attracting tremendous attention for its pure manganese Kagome lattice which can host flat bands and topologically non-trivial Dirac cones at K and K' points of its hexagonal Brillouin zone.[12–19] In magnetic materials, the structure of these topological bands leads to a variety of exotic phenomena such as large anomalous Hall effect and Nernst effect that are closely related to Berry curvature near Fermi surface. $TbMn_6Sn_6$ is one of the RMn_6Sn_6 (R = rare earth, Sc, Y, Gd–Tm, Lu) family, where the rare earth atoms' hexagonal planes (H) and manganese Kagome planes (K) stack alternatively to form K–H–K–K–H–K structure with tin layers in between them. Different from other Kagome-magnetic compounds, the material has a ferromagnetic ground state (T_C = 423 K) formed by antiferromagnetic Tb and Mn layers.[20–22] Below 300 K, it has strong out-of-plane magnetization with all the spin of Tb and Mn parallel to the c axis with magnetic momentum of 8.6 μ_b and 2.5 μ_b, respectively.[23] It has a rather large coercive field of 1.1 T. The time-reversal symmetry breaking and strong SOC yield a unique gapped Chern phase suitable for investigating topological fermions and their interaction with magnetization.[24,25] A recent report suggests superconducting states emerges at the interface between $TbMn_6Sn_6$ and a normal metal at extremely low temperatures, which might be a candidate for spin triplet superconducting.[14]

In this Letter, we demonstrate the performance of our MOKE system by studying the Kerr rotation angle of $TbMn_6Sn_6$. Because our measurement temperature is much lower than T_C, the magnetic moments of Tb and Mn remain antiferromagnetic aligned and flip together in external magnetic field. In the MOKE measurement, the

†These authors contributed equally to this work.
*Corresponding authors. Email: wanghe@cnu.edu.cn; liuyang02@pku.edu.cn
© 2024 Chinese Physical Society and IOP Publishing Ltd

interaction between optical polarization and magnetism is mediated by the Hall conductance of the freely moving carriers, inter-band transitions, and the dielectric constant of the full-filled bands. Therefore, we can extrapolate information of the material's Chern band properties and may inspire related future studies, for example, magnetic topological insulator and spin triplet superconductor.

The interferometer and its low-temperature mounting in a dilution fridge is shown in Fig. 1. Our ultra-low temperature MOKE measure system is an all-fiber Sagnac interferometer using linear polarization maintaining (PM) fibers where two orthogonal modes have perpendicularly linear-polarized electric field. These two modes have different effective refractive indices and are usually referred to as fast and slow axes of light. We use an ASE (amplification of spontaneous emission) broadband light source centered at wavelength 1550 nm. A polarizer evenly distributes the light into the fast and slow axes. The light in the fast (slow) axis becomes CW (CCW) light after passing through the $\lambda/4$ plate whose optical axis is 45° from the fast and slow axis. It then reflects from the sample surface and becomes CCW (CW) polarized with an additional phase. The returned light propagates through the same fiber in the slow (fast) axis and interferes at the polarizer. The total phase difference between the two light paths other than modulation is zero except for the magnetic-optical Kerr angle $2\theta_{\rm K}$ acquired at the sample surface. In order to improve measurement accuracy, we use an electro-optical phase modulator (EOM) to introduce a phase modulation. The light accumulate $+\varphi_{\rm M}(t)$ phase difference when it first passes through the EOM, and $-\varphi_{\rm M}(t+\tau)$ on its return path; τ is the delay time determined by the fiber length. We use a 2-m-long fiber and 25 MHz modulation frequency in our MOKE system so that $\omega\tau = \pi$ and $+\varphi_{\rm M}(t) = -\varphi_{\rm M}(t+\tau)$ to maximize the modulation efficiency. The total phase difference between the path is $+2\varphi_{\rm M}(t) + 2\theta_{\rm K}$ and the Kerr signal can be derived as[11]

$$\theta_{\rm K} = \frac{1}{2}\arctan\frac{V_1 \cdot J_2(\phi_{\rm M})}{V_2 \cdot J_1(\phi_{\rm M})},$$

where V_1 and V_2 are the first and second harmonic components in the optical signal, J_N is the N-th order Bessel function of the first kind, and $\phi_{\rm M}$ is the modulation depth.

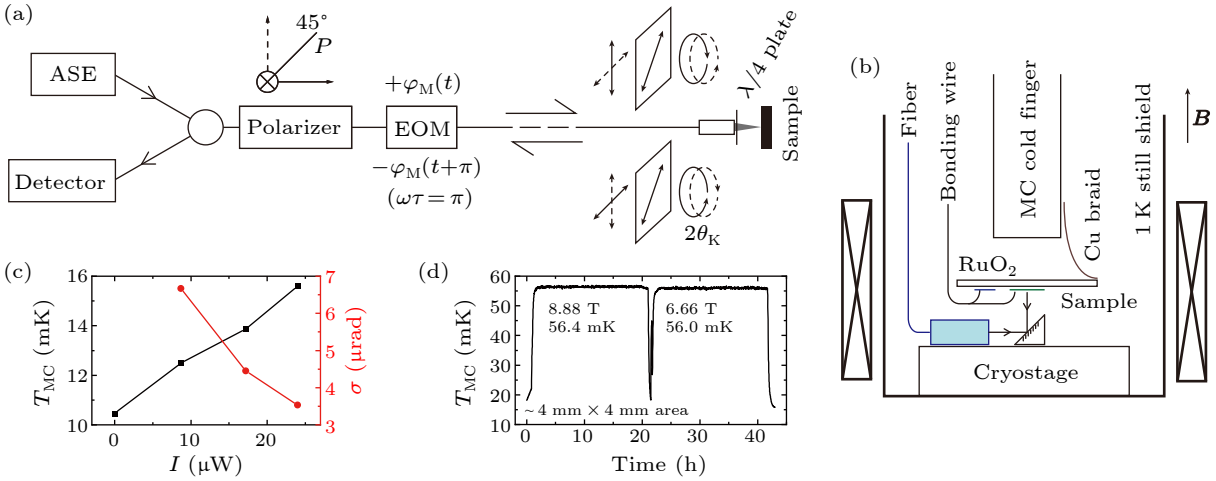

Fig. 1. (a) Schematic of the fiber interferometer. Its two arms are the orthogonal polarization modes, i.e., horizontal and vertical in the figure, of the polarization-maintaining fiber. The dashed and solid lines are two beams of light which propagate in two fiber modes. These two beams have the same light path, which cancels the majority of drift so that the interference is only sensitive to the nonreciprocal Kerr signal from the sample. (b) Schematic drawing of the low-temperature sample stage installed in the dilution fridge. The sample holder is cooled by the MC plate's cold finger and thermally isolated from the rest of the system. Samples and a RuO_2 thermometer are attached to the holder upside-down and can be further cooled by bonding wires from the MC plate. The sample is in the center of fridge's superconducting magnet. The piezo scanner is installed on the still shield. A fiber Grin lens moving with the piezo-scanner focuses the light onto a spot of about 15 μm. (c) The temperature of the MC plate and the noise level of our system with different light intensities applied to the sample. The lowest $T_{\rm MC} = 10.5$ mK when the light is off. (d) The temperature of the MC plate when the scanning stage is working. A ∼4 mm × 4 mm area was scanned twice at 8.88 T and 6.66 T, respectively. After the scan finish, the temperature becomes quickly down to ∼15 mK since the light is still on.

This all-fiber zero-loop interferometer and its immunity to thermal gradient, twist, etc. allow simple installation in the dilution refrigerator. The 2-m-long optical fiber gets into the fridge by a vacuum feedthrough and is fixed by Polyimide vacuum tape when going down to the sample space. A self-focus Grin lens focuses the light into a nearly 15 μm spot on the sample. The non-PM lens is perpendicular to the magnetic field to reduce its Faraday effect, and light will be reflected to the sample by a piece of Au-coated Si wafer. To achieve mK temperature optical and scanning measurement, we need to overcome three major problems. First, when scanning, the piezo stage can generate heat that will vaporize all the mixture in the mixing chamber (MC) and stop the dilution cooling circulation. Therefore, we must redesign the sample stage and separately mount the scanning stage to the still

shield, see Fig. 1(b). The still stage has mK-level cooling power, and moderate increase of still temperature does not affect the mixing chamber temperature by a lot. Second, since we cannot adjust the optical alignment after closing the fridge, we designed a reliable optical mount [omitted in Fig. 1(b)] which barely change during the cooling process from 300 K to 1 K. Third, to cool down the sample to mK temperature, we carefully design the thermal connection, optimize the electronic circuits, and minimize the optical power. As shown in Fig. 1(b), the sample holder is installed onto a copper plate which is thermally anchored to the MC plate's cold finger with a Cu braid. The customized cold finger takes the place of the original puck for quick loading on the MC plate. The copper plate is the movable part of the optical mount and is fixed to the mount by springs and screws for fine adjustment. The springs and screws only have point contact with the copper plate, which makes the plate nearly adiabatic to the still shield. In this case, the sample can only be heat up by radiation from the scanning stage and the shield. The low resistance wires for actuating the scanning stage are well thermally anchored at each plate of the fridge to minimize the heat flow step by step. Bonding wires from the MC plate give direct cooling power to the sample. To balance the sample temperature and noise performance, we tried to vary the light intensity as shown in Fig. 1(c), in which the data for standard deviation σ is measured by lock-in with 300 ms time constant. We install an RuO_2 resistor on the sample holder to monitor the sample temperature change. However, for consistency and accuracy, we quote the calibrated MC temperature instead in Fig. 1(c). Also, the performance of the scanning stage was tested as shown in Fig. 1(d). The non-magnetic piezo stage can work up to 12 T magnetic field and can scan imaging $\sim 4\,\text{mm} \times 4\,\text{mm}$ area in 20 h. During the scanning, the MC plate is heated up to ~ 56 mK, which is sufficiently low for our current studies. In summary, we are able to resolve $\sim 0.2\,\mu\text{rad}$ with 400 s average and scan images for mm-size samples while keeping its temperature below ~ 100 mK.

We use our setup to study the Kerr effects of $TbMn_6Sn_6$ at an ultra-low temperature and room temperature (RT, ~ 300 K) in Fig. 2. At about 200 mK, a clear ferromagnetic hysteresis loop in the Kerr signal appears when sweeping magnetic field parallel to c axis after zero-field cooling. The coercive field is asymmetric at 0.4–0.6 T with exchange bias of ~ 0.2 T when trained by 2 T magnetic field, and increases to ~ 1.2 T after trained by 12 T. This square shape hysteresis loop is closely related to the saturation magnetic momentum flip. An out-of-plane ferrimagnetic ground state is formed with the bound electrons in Mn $3d$ and Tb $4f$ orbits with antiparallel spin and may lead to this flip. In addition, we observe a linear θ_K vs B relation whose slope $d\theta_K/dB$ has an opposite sign with the ferromagnetic jump during the up/down sweep of B. At RT, we study the sample using a similar interferometer and a coil with maximum field 0.6 T. The ferromagnetic hysteresis is weaker and the slope becomes positive.

Several mechanisms may contribute to a finite Kerr angle. Firstly, the electric field of the light drives the bound electrons from its equilibrium position and induces a finite dipole moment $\boldsymbol{P}$ perpendicular to the light wave vector $\boldsymbol{k}$. The magnetic field along $\boldsymbol{k}$ direction induces a Lorentz force so that the dielectric tensor has a finite off-diagonal term δ.[26] The θ_K induced by this process is proportional to $\boldsymbol{B}$ with positive $d\theta_K/dB$ in few exceptions. Secondly, the finite conductivity of unbound electrons/holes contributes to the imaginary part of the dielectric constant.[27] The phase difference between the two circular polarized incident light modes is proportional to the Hall conductance. The polarity of $d\theta_K/dB$ will be positive if the major carriers are electrons, and will be negative if holes dominate the transport conductivity. Thirdly, the spin polarization of the charged particles usually induces a finite Kerr effect through the spin-orbit coupling and selection rule for the interband transitions.[6]

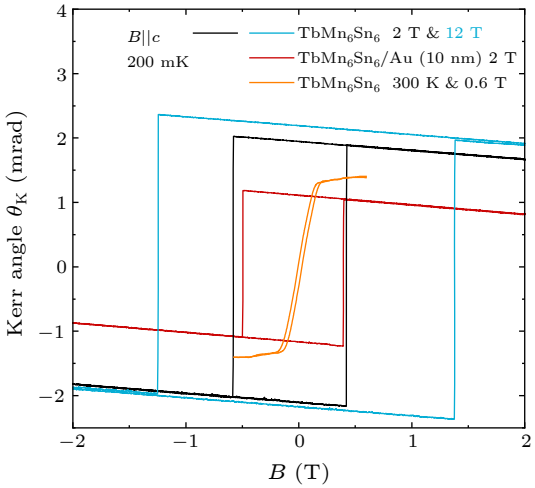

Fig. 2. MOKE hysteresis loop of $TbMn_6Sn_6$ surface with/without Au coating layer. At ~ 200 mK, coercive fields are almost the same and both have an exchange bias of ~ 0.2 T, when sweep between ± 2 T magnetic field, and increase to ~ 1.2 T after experiencing 12 T. Besides the ferromagnetic change of θ_K, there is a linear part of Kerr angle that has a negative slope vs B caused by paramagnetic free holes in $TbMn_6Sn_6$. At RT, the sample (orange line) has smaller hysteresis and electron-like positive slope vs B.

In $TbMn_6Sn_6$, we observe a linear dependence of θ_K vs B at the large magnetic field with a large negative slope. A previous scanning-tunneling-microscope study shows that the Fermi energy of $TbMn_6Sn_6$ lies in the hole band at about 134 meV below the charge neutral point of its Dirac cone.[12] As a result, holes are the majority of free carriers and will generate a negative Kerr signal compare to the bound electrons. The hole density of each Mn sublayer is about $1.16 \times 10^{12}\,\text{cm}^{-2}$. The Chern gap $\Delta = 34$ meV modifies the linear dispersion so that the effective mass $m^* = E_D/v^2 = 0.13m_0$, where $v = 4.2 \times 10^5$ m/s is the Dirac velocity.[12] Therefore, the $d\theta_K/dB = 0.5$ mrad/T suggests that the penetration depth of the reflected light is about 10 atomic layers, which is consistent with our expectation.[27]

On the other hand, the θ_K jump at the coercive field is a direct result of the discontinuous of magnetic mo-

ment. It is interesting to note that this flip is positive while $d\theta_K/dB < 0$, suggesting that these two procedures have different origins. In their report, Yin *et al.* suggests that the the electronic states near the Fermi energy are spin-polarized.[12] In that case, one would expect a flipping of these electron spin, which may result in a large θ_K caused by spin-orbit coupling. Although a careful theoretical study is out of our scope here, our data is clearly consistent with a spin-polarized system. For different behavior of the sample at room and base temperature, the relative weak ferromagnetism ground state and the high kinetic energy at RT may be the reason.

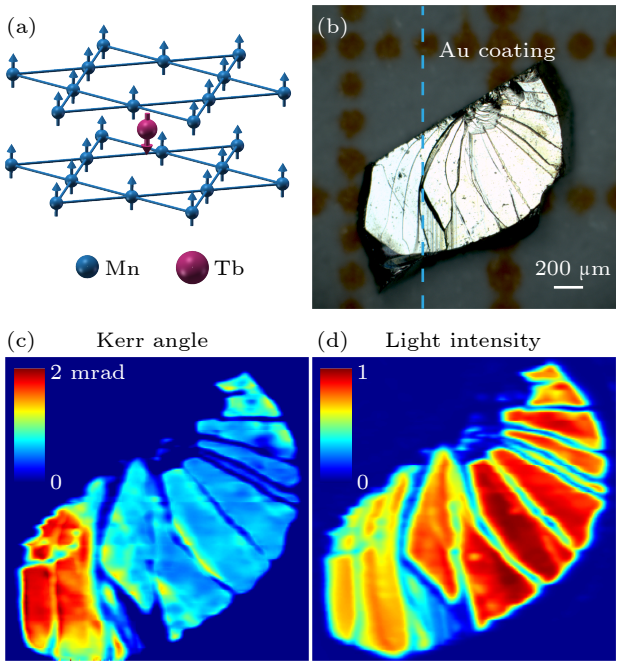

Fig. 3. (a) Magnetism in $TbMn_6Sn_6$. Manganese (blue) atoms form Kagome lattice, and together with terbium (red) with antiparallel spin form ferrimagnetic ground state. The Sn atoms are omitted for simplicity since it has no net magnetic momentum. (b) Picture of newly cleaved $TbMn_6Sn_6$ sample with its right half coated with Au (10 nm). [(c), (d)] The Kerr signal and normalized light intensity at $B = 0$ T back from 2 T (along c axis), respectively. Temperature during scanning is $\sim$100 mK.

MOKE is a powerful tool for studying film-like systems. We integrate a piezo-scanner in our setup so that we can take MOKE images at $\sim$100 mK and up to 12 T magnetic field. Figures 3(c) and 3(d) show MOKE signals and the normalized reflected light intensity. The images are similar to the sample photo taken by a microscope at room temperature: plaques of smooth surface separated by steps. The surface to the right of the dashed line in Fig. 3(b) is coated with 10 nm Au and has better reflectivity. The left part, two plateaus more specifically, is bare $TbMn_6Sn_6$. Beside the unevenness of light intensity caused by imperfect cleavage surface, defects of Au coating and rough sample edges, the Au-coated surface does have a slightly higher reflectivity. The Kerr signal in Fig. 3(c) is measured at zero fields after sweep back from +2 T. We can clearly distinguish the two parts with/without Au, in which the magnitude of the Kerr angle is consistent with Fig. 2. In each region, Kerr angle is quite homogeneous despite the fluctuating light intensity. We can further confirm that 10 nm Au coating cannot completely screen light from penetrating into the $TbMn_6Sn_6$.

An interesting fact is that the negative slope values on the Au surface and bare $TbMn_6Sn_6$ surface are nearly same when the Kerr angle discontinuity differs significantly. It is arguably due to the contribution of θ_K from exciting electrons from the ferromagnetic Chern band to the conduction band is related to the reduced intensity of light penetrating through the Au layers. A precise numerical model should include electron motion as well as the electromagnetic field in all layers, and include contributions from the Hall effect, interband transitions, etc., which is far beyond the scope of this manuscript.

To sum up, we have installed a high-frequency phase modulated all-fiber Sagnac interferometer into a dilution refrigerator to build a magneto-optical Kerr effect measure system specialized at mK temperature and high magnetic field. We demonstrate its performance by investigating the ferromagnetic ground state of a Kagome compound $TbMn_6Sn_6$. The Kerr result has a clear hysteresis loop consistent with the transport anomalous Hall effect and minus slope vs B origins from the free hole carriers that have strong SOC in the Dirac cone. Also, we scan the sample to get a rather high-resolution image of the Kerr signal distribution. The Kerr signal acquired through 10 nm Au coating, which is a typical thickness for gate or contact, is tested. The signal is about half of direct detecting and still much larger than our noise level of 0.2 μrad, making it possible for further research involving gate voltage control and interface states.

Acknowledgement. The work at PKU was supported by the National Key Research and Development Program of China (Grant Nos. 2021YFA1401900, 2019YFA0308403, and 2018YFA0305604), the Innovation Program for Quantum Science and Technology (Grant Nos. 2021ZD0302602 and 2021ZD0302403), the National Natural Science Foundation of China (Grant Nos. 92065104, 12074010, and 11888101), and Capacity Building for Sci-Tech Innovation-Fundamental Scientific Research Funds (Grant Nos. 20530290057 and KM202010028014). The $TbMn_6Sn_6$ sample is supplied by Jian Wang at the International Center for Quantum materials, Peking University and He Wang at Capital Normal University.

References

[1] Xia J, Schemm E, Deutscher G, Kivelson S A, Bonn D A, Hardy W N, Liang R, Siemons W, Koster G, Fejer M M, and Kapitulnik A 2008 *Phys. Rev. Lett.* **100** 127002

[2] Xia J, Siemons W, Koster G, Beasley M R, and Kapitulnik A 2009 Phys. Rev. B **79** 140407

[3] Schemm E R, Gannon W J, Wishne C M, Halperin W P, and Kapitulnik A 2014 *Science* **345** 190

[4] Thomas S, Kuiper B, Hu J, Smit J, Liao Z, Zhong Z, Rijnders G, Vailionis A, Wu R, Koster G, and Xia J 2017

Phys. Rev. Lett. **119** 177203
[5] Sarkar T, Wei D S, Zhang J, Poniatowski N R, Mandal P R, Kapitulnik A, and Greene R L 2020 *Science* **368** 532
[6] Pershan P S 1967 *J. Appl. Phys.* **38** 1482
[7] Kapitulnik A 2015 *Physica B* **460** 151
[8] Zhao L, Lin W, Chung Y J, Gupta A, Baldwin K W, Pfeiffer L N, and Liu Y 2023 *Phys. Rev. Lett.* **130** 246401
[9] Sun H M, Liu Y Z, Huang D Q, Fu Y, Huang Y, He M Y, Luo X M, Song W J, Liu Y, Yu G Q, and He Q L 2023 *Commun. Phys.* **6** 222
[10] Xia J, Maeno Y, Beyersdorf P T, Fejer M M, and Kapitulnik A 2006 *Phys. Rev. Lett.* **97** 167002
[11] Fried A, Fejer M, and Kapitulnik A 2014 *Rev. Sci. Instrum.* **85** 103707
[12] Yin J X, Ma W, Cochran T A, Xu X, Zhang S S, Tien H J, Shumiya N, Cheng G, Jiang K, Lian B, Song Z, Chang G, Belopolski I, Multer D, Litskevich M, Cheng Z J, Yang X P, Swidler B, Zhou H, Lin H, Neupert T, Wang Z, Yao N, Chang T R, Jia S, and Zahid Hasan M 2020 *Nature* **583** 533
[13] Zhang H D, Koo J, Xu C Q, Sretenovic M, Yan B H, and Ke X L 2022 *Nat. Commun.* **13** 1091
[14] Wang H, Liu Y Z, Gong M, Jiang H, Gao X Y, Ma W L, Luo J W, Ji H R, Ge J, Jia S, Gao P, Wang Z Q, Xie X C, and Wang J 2023 *Nat. Commun.* **14** 6998
[15] Tang E, Mei J W, and Wen X G 2011 *Phys. Rev. Lett.* **106** 236802
[16] Cai G H, Jiang Y T, Zhou H, Yu Z, Jiang K, Shi Y G, Meng S, and Liu M 2023 *Chin. Phys. Lett.* **40** 117101
[17] Lee Y, Skomski R, Wang X, Orth P P, Ren Y, Kang B, Pathak A K, Kutepov A, Harmon B N, McQueeney R J, Mazin I I, and Ke L 2023 *Phys. Rev. B* **108** 045132
[18] Li R S, Zhang T, Ma W L, Xu S X, Wu Q, Yue L, Zhang S J, Liu Q M, Wang Z X, Hu T C, Zhou X Y, Wu D, Dong T, Jia S, Weng H M, and Wang N L 2023 *Phys. Rev. B* **107** 045115
[19] Xu X T, Yin J X, Ma W L, Tien H J, Qiang X B, Reddy P V S, Zhou H, Shen J, Lu H Z, Chang T R, Qu Z, and Jia S 2022 *Nat. Commun.* **13** 1197
[20] Hu J F, Wang K Y, Hu B P, Wang Y Z, Wang Z, Yang F, Tang N, Zhao R, and Qin W 1995 *J. Phys.: Condens. Matter* **7** 889
[21] Zajkov N K, Mushnikov N V, Bartashevich M I, and Goto T 2000 *J. Alloys Compd.* **309** 26
[22] Ma W L, Xu X T, Yin J X, Yang H, Zhou H B, Cheng Z J, Huang Y, Qu Z, Wang F, Hasan M Z, and Jia S 2021 *Phys. Rev. Lett.* **126** 246602
[23] Riberolles S X M, Slade T J, Dally R L, Sarte P M, Li B, Han T, Lane H, Stock C, Bhandari H, Ghimire N J, Abernathy D L, Canfield P C, Lynn J W, Ueland B G, and McQueeney R J 2023 *Nat. Commun.* **14** 2658
[24] Wenzel M, Tsirlin A A, Iakutkina O, Yin Q, Lei H C, Dressel M, and Uykur E 2022 *Phys. Rev. B* **106** L241108
[25] Riberolles S X M, Slade T J, Abernathy D L, Granroth G E, Li B, Lee Y, Canfield P C, Ueland B G, Ke L, and McQueeney R J 2022 *Phys. Rev. X* **12** 021043
[26] Argyres P N 1955 *Phys. Rev.* **97** 334
[27] Moss T S 1962 *Phys. Status Solidi B* **2** 601